Hindawi
International Journal of Antennas and Propagation
Volume 2021, Article ID 8699512, 10 pages
https://doi.org/10.1155/2021/8699512

Research Article

Incoherent Integration Detection Method of Airborne Phased Array Radar in a Multipath Environment

Yili Hu, Yongbo Zhao, and Sheng Chen

National Lab of Radar Signal Processing, Xidian University, Xi'an 710071, China

Correspondence should be addressed to Yongbo Zhao; ybzhao@xidian.edu.cn

Received 17 July 2021; Revised 23 November 2021; Accepted 25 November 2021; Published 15 December 2021

Academic Editor: Atsushi Mase

Airborne phased array radar (PAR) suffers from multipath problems when flying over a calm sea surface. The existence of a multipath phenomenon will cause the electromagnetic echo of the same target to be reflected back to the airborne PAR from two paths, namely, direct path (DP) and multipath. Compared with the ground-based radar, the target echo received by airborne PAR in the multipath environment has two important characteristics: one is that the DP signal and the multipath signal exist in different range bins, and the other is that the radar cross section (RCS) in the DP direction may be smaller than that in the multipath direction. Considering these two characteristics, this paper first proposes a target pairing algorithm for matching the DP range and multipath range of the same target in signal detection, and then, combined with the cell-averaging constant false alarm rate (CA-CFAR) detection model, an incoherent integration detection method for airborne PAR in the multipath environment is proposed. In the target pairing process, the geometric structure relationship of the airborne PAR model can be fully utilized. After a successful target pairing process, the energy of the multipath signal will be incoherently accumulated into the corresponding DP range bin, so as to improve the probability of DP range bin data passing the detection threshold. In essence, the proposed method makes full use of multipath energy to improve the detection capability of airborne PAR in the multipath environment. Finally, the detection probability of the proposed method is given, and the detection performance is analyzed.

1. Introduction

Airborne phased array radar (PAR) is a special radar system that places the antenna elements on the airborne platform. It is tactically important because of its wide field of vision, good manoeuvrability, and simultaneous detection capability of ground and air targets. Compared with a ground-based radar, the airborne PAR suffers from more complex clutter and interference, but when combined with the system characteristics of the airborne PAR, many solutions have been proposed to deal with these problems [1–6].

Multipath is caused by the high reflectivity of the sea surface at microwave frequencies. Multipath causes multiple propagation paths between the radar and the target, which usually implies that the target is illuminated from two directions and that the radar receives the return energy from two directions [7–9]. Airborne PAR is prone to multipath phenomena in special reflection scenarios such as calm sea surfaces [10–12]. When airborne PAR suffers from multipath problems, most research studies are focused on multipath suppression of clutter and interference [13–16] and parameter estimation [17–20]. In the airborne PAR, the direct path (DP) signal and the multipath signal are not in the same range bin. Therefore, the data in the DP range bin can be directly used for signal detection [21–23]. Obviously, these methods result in a waste of multipath signal energy and cannot fully utilize the targets' multipath energy for signal detection. In [22], the radar detection problem is devised as a constrained generalized likelihood ratio test in a multipath diffuse reflection environment, and the proposed method still has the property of the constant false alarm rate (CFAR). In [23], an adaptive constrained generalized likelihood ratio test method is proposed to find range diversity targets under diffuse reflection, and the main process is that in each range bin of the original data, the echo data is transformed into the covariance of the secondary data sample, but the detection performance of the method in heterogeneous echo data needs to be improved. In general,

the methods in [22, 23] do not make full use of the energy of multipath, and the radar cross section (RCS) characteristics of different path echoes of airborne PAR in a multipath environment are not analyzed.

In this paper, the synthetic multipath reflection coefficient (SMRC) of airborne PAR is analyzed. Based on the analysis of SMRC, this paper systematically summarizes the power relationship between the DP signal and the multipath signal of airborne PAR and clearly emphasizes a special multipath phenomenon; that is, the multipath power of airborne PAR in the multipath environment may be greater than the DP power. Furthermore, aiming at the multipath model of airborne PAR, this paper proposes a new signal detection process to improve the detection probability by incoherent integration of multipath energy. Specifically, a target pairing algorithm for matching the DP range and multipath range of the same target is proposed first, and then the corresponding incoherent integration detection method is carried out after a successful target pairing process. Finally, the detection probability expression of the proposed incoherent integration detection method is given.

The remainder of this paper is organized as follows: the analysis of the multipath model and the SMRC of airborne PAR in a multipath environment are given in Section 2; the proposed incoherent integration detection method is described in Section 3; and Section 4 analyzes the performance of the proposed method. Then, summarizing remarks are given in Section 5.

2. Signal Model Analysis of Airborne Phased Array Radar in a Multipath Environment

2.1. Analysis of Multipath Model. The echo model of the airborne PAR in a multipath environment is shown in Figure 1.

In Figure 1, R_e is the radius of the earth, H is the platform height of airborne PAR, H_t is the height of the target, θ_d is the angle between the horizontal and the received DP, θ_i is the angle between the horizontal and the received multipath, R_d is the DP range, $R_i = R_1 + R_2$ is the multipath range, and h_b is the height of the reflection area. Note that the multipath phenomenon of airborne PAR is mainly caused by strong specular reflection when flying over a calm sea surface, so only the multipath of the elevation direction needs to be considered [24].

According to the echo characteristics of the airborne radar, the range difference between the DP signal and the multipath signal is very large, causing the DP signal and multipath signal to not be within the same range bin. Thus, from Figure 1, the angle θ_B between the DP signal and the multipath signal is large, so that the RCS of the DP signal is possible to be smaller than that of the multipath signal, resulting in the echo power of the multipath signal being greater than that of the DP signal. If the power of the multipath signal is not used in signal detection, the multipath return energy will be wasted.

Note that in the ground-based radar, the angle θ_B is very small (usually less than 0.5°), so it is often considered that the

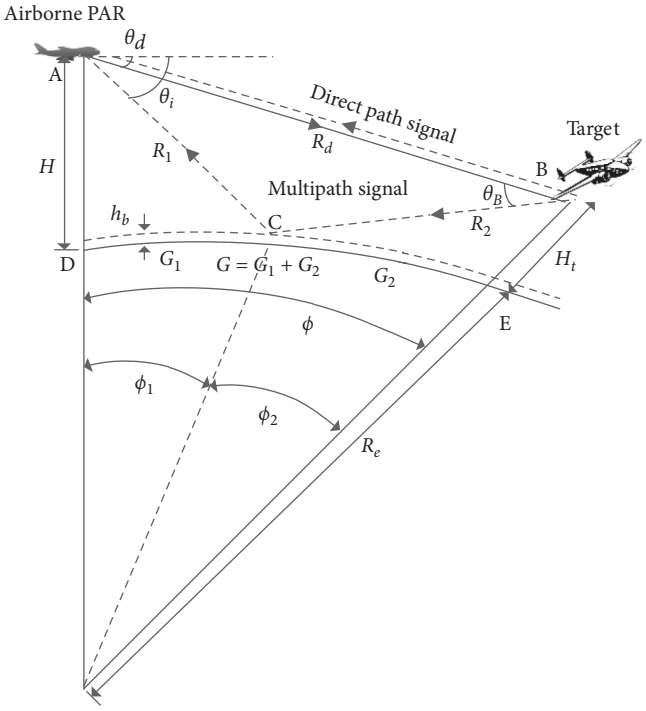

Figure 1: The signal model of airborne PAR in a multipath environment.

RCS values of the DP signal and the multipath signal in the ground-based radar model are approximately equal. The relationship between the RCS values of the DP signal and the multipath signal is an important difference of echo energy between airborne PAR and ground-based radar in the multipath environment.

The simplified signal model of Figure 1 is shown in Figure 2.

From Figure 2, the multipath range R_i is greater than the DP range R_d. The range difference between R_i and R_d is a function of the radar's waveform parameters and the geometry model of the reflection surface. Generally, as long as the platform height H of the airborne PAR model is not very low (i.e., $H \geq 1$km), R_d and R_i are in different range bins. Therefore, this paper defaults that the DP range and multipath range are in different range bins.

2.2. The Modeling and Analysis of the Synthetic Multipath Reflection Coefficient. Due to the large angle θ_B of the airborne PAR multipath model shown in Figure 2, the RCS values of the DP signal and the multipath signal are no longer approximately equal. Therefore, it is important to study the echo power of the DP signal and the multipath signal.

To analyze the power of signals from different paths of the same target in a multipath environment, the concept of the synthetic multipath reflection coefficient (SMRC) will be introduced. The SMRC reflects the amplitude ratio of the multipath signal to the DP signal.

The echo power P_{o_d} of the DP signal and the echo power P_{o_i} of the multipath signal can be expressed as follows:

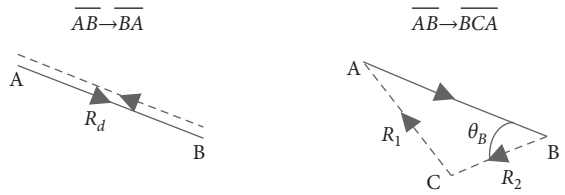

Direct path (DP) signal

Multipath signal

A:airborne radar
B:target
C:reflection surface

Figure 2: The simplified signal model in a multipath environment.

$$P_{o\_d} = \frac{\left(P_{t,d}G_{t,d}G_{r,d}\lambda^2\sigma_d\right)}{\left((4\pi)^3R_d^4\right)}, \tag{1}$$

$$P_{o\_i} = \frac{\left(P_{t,i}G_{t,i}G_{r,i}\lambda^2\sigma_i\right)}{\left((4\pi)^3R_i^4\right)}, \tag{2}$$

where λ is wavelength, σ_d and σ_i are the RCS of the DP signal and the multipath signal, respectively, transmitting power $P_{t,d} = P_{t,i}$, transmitting gain $G_{t,d} = G_{t,i}$, and the reflection attenuation coefficient $\varepsilon \le 1$, that is, $G_{r,i} = \varepsilon G_{r,d}$. The SMRC ρ can be represented as follows:

$$\rho^2 = \frac{P_{o\_i}}{P_{o\_d}} = \varepsilon\frac{\left(\sigma_iR_d^4\right)}{\left(\sigma_dR_i^4\right)}. \tag{3}$$

According to equation (3), the SMRC ρ is related to the RCS, reflection attenuation coefficient ε, and ranges of the DP signal and the multipath signal.

In a ground-based radar, the multipath phenomenon is easy to occur when the ground-based radar measures the height of a low-elevation target [25, 26], where σ_i/σ_d and R_d^4/R_i^4 are approximately equal to 1. Therefore, according to equation (3), the SMRC of the ground-based radar is mainly determined by the reflection attenuation coefficient ε. However, in the airborne PAR multipath model, σ_i/σ_d and R_d^4/R_i^4 are no longer approximately equal to 1, and their specific ratio values should be considered in combination with the actual radar system parameters. Note that according to equation (3), the SMRC amplitude $|\rho|$ may be greater than 1, which means that compared with the ground-based radar, airborne PAR has a special multipath phenomenon; that is, multipath power may be greater than the DP power.

In the process of signal detection, the DP range R_d and the multipath range R_i can be obtained by pulse compression (PC) operation. Through the range difference $\Delta R = R_i - R_d$ between R_i and R_d, the relative time delay difference $\Delta\tau$ can be expressed as follows:

$$\Delta\tau = \tau_{ii} - \tau_{dd} = \frac{\left(R_i - R_d\right)}{c}, \tag{4}$$

where $\tau_{dd} = 2R_d/c$, $\tau_{ii} = (R_d + R_i)/c$, and $c = 3\times10^8 m/s$. The large range difference ΔR between the DP signal and the multipath signal results in large relative time delay $\Delta\tau$, that is, $\Delta\tau > 1/2f_s$, where f_s is the sampling frequency. Therefore, the complex envelopes of the DP signal and the multipath signal will be misalignment, leading to the failure of the joint steering vector class method [27] for signal detection.

3. The Proposed Incoherent Integration Detection Method

3.1. The Proposed Method. The CFAR is a common signal detection method. In this section, the cell-average CFAR (CA-CFAR) [28] detection model will be used. Figure 3 shows a flowchart of the proposed incoherent integration detection method for airborne PAR in a multipath environment.

In Figure 3, system parameters mainly refer to the platform height H and the elevation wave position in the fast time data process when the radar transmits a burst of pulses. Sampling echo data refers to the discretized of echo data sampled by the receiving antennas after passing through A/D components. The MTD refers to the moving target detection, and it is also a classic Doppler filtering operation [29], which can effectively suppress interference and sea clutter. The PC refers to the pulse compression which can obtain the target ranges. The process of target pairing is to ensure that the ranges of the DP signal and the multipath signal from the same target can be paired. Note that, in the process of data from PC to target pairing, the operation of plot centroid [24] is required to ensure that the targets are roughly found. However, when the noise amplitude is much larger than the signal amplitude, the rough found target cannot be obtained by the plot centroid operation. In order to avoid the noise becoming the false target and affecting the success probability of signal detection, the proposed method in Figure 3 is not suitable for application at a very low signal-to-noise ratio (SNR).

The processes of target pairing and incoherent integration are the most important differences between the proposed method in Figure 3 and existing methods [13–16, 21–23]. Target pairing is an important process in Figure 3. The DP range R_d and the multipath range R_i can be obtained after PC, but when we are detecting targets, we cannot directly confirm that R_d and R_i correspond to the two different path ranges of the same target. Therefore, after PC, we need to perform the target pairing process to match the DP range and the multipath range of the same target.

In the airborne PAR system, some priori information can be used in the target pairing process, especially the platform height H and the elevation wave position $\widetilde{\theta}_d$.

The specific target pairing process is as follows: firstly, the system parameters H and $\widetilde{\theta}_d$ are obtained, and then, the range set of the rough found targets $R = [R_1, \ldots, R_k, \ldots, R_K]$ can be obtained after PC, where $k = 1, 2, \ldots, K$, K is the number of rough found targets. Finally, according to the system parameters and one of the range value $R_k \in$ R, the multipath range R_{k2} can be calculated by using the geometric structure relationship in Figure 1.

Furthermore, the specific calculation process of the multipath range R_{k2} can be as follows: the revised platform

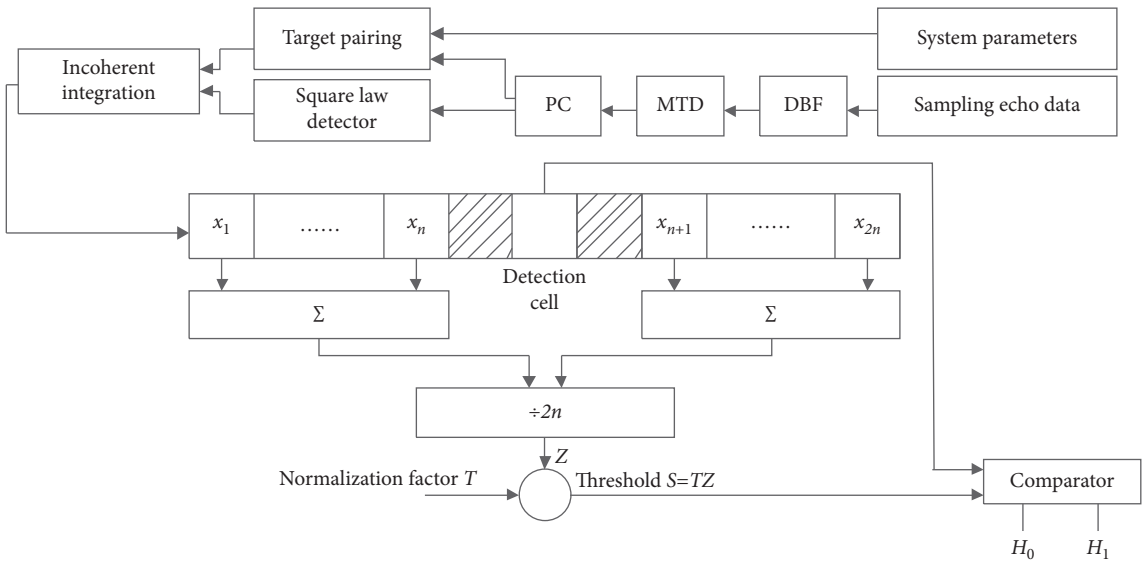

Figure 3: The proposed incoherent integration detection model.

height is $\overline{H} = H - h_b$, the revised radius of the earth is $\overline{R}_e = R_e + h_b$, and then, assuming that the DP range is R_k in the range set R for target pairing, the target height H_t can be represented as follows:

$$H_t = \sqrt{R_k^2 + (\overline{R}_e + \overline{H})^2 - 2R_k(\overline{R}_e + \overline{H})\cos\left(\widetilde{\theta}_d + \frac{\pi}{2}\right)} - \overline{R}_e. \tag{5}$$

The angle ϕ in Figure 1 can be obtained as follows:

$$\phi = \cos^{-1}\frac{(\overline{R}_e + \overline{H})^2 + (\overline{R}_e + H_t)^2 - R_k^2}{2(\overline{R}_e + \overline{H})(\overline{R}_e + H_t)}. \tag{6}$$

The length G of the curve in Figure 1 can be represented as follows:

$$G = \overline{R}_e\ \phi. \tag{7}$$

And then, ϕ_1 and ϕ_2 can be represented as follows:

$$\phi_1 = \frac{G_1}{\overline{R}_e}, \tag{8}$$

$$\phi_2 = \frac{(G - G_1)}{\overline{R}_e}, \tag{9}$$

where

$$G_1 = \frac{G}{2} - \eta\ \sin\frac{\xi}{3}, \tag{10}$$

$$\eta = \frac{2}{\sqrt{3}}\sqrt{\overline{R}_e(\overline{H} + H_t) + \frac{G^2}{4}}, \tag{11}$$

$$\xi = \sin^{-1}\frac{2\overline{R}_e\ G(H_t - \overline{H})}{\eta^3}. \tag{12}$$

Finally, the multipath range R_{k2} can be represented as follows:

$$\begin{cases} R_{k2} = R_{k\_1} + R_{k\_2}, \\ R_{k\_1} = \sqrt{\overline{R}_e^2 + (\overline{R}_e + \overline{H})^2 - 2\overline{R}_e(\overline{R}_e + \overline{H})\cos\ \phi_1}, \\ R_{k\_2} = \sqrt{\overline{R}_e^2 + (\overline{R}_e + H_t)^2 - 2\overline{R}_e(\overline{R}_e + H_t)\cos\ \phi_2}. \end{cases} \tag{13}$$

If R_{k2} is also in the target range set R, it can be considered that the DP range R_k and the multipath range R_{k2} are successfully paired. If R_{k2} is not in the target range set R, it means that the target at the range R_k has no multipath echo or the multipath echo energy is too weak to be detected.

Once the DP range of the target is successfully paired with its multipath range, we can perform the incoherent integration process. If the snapshot data of the DP signal and the multipath signal are X_d and X_i, respectively, then the snapshot data X_{di} at the DP range bin after incoherent integration is as follows:

$$|X_{di}|^2 = |X_d|^2 + |X_i|^2. \tag{14}$$

Thus, the power of the DP range bin after incoherent integration is $P_{o\_di} = (1 + |\rho|^2)P_{o\_d}$, where P_{o_d} is the power of the DP signal before incoherent integration.

Note that if the platform height is very low and the airborne PAR system is oversampling, the DP range and multipath range may also be in the same range bin. But the proposed incoherent integration method can still use equations (5)–(13) to calculate the multipath range in the target pairing process. If the calculated range difference between the multipath range and the DP range is within a range bin, the incoherent integration of equation (14) is still valid, and the proposed method can still ensure that the multipath echo energy can be fully utilized for signal detection.

3.2. Analysis of Detection Probability of the Proposed Method. The decision criteria of CA-CFAR is as follows:

$$\begin{cases} D > TZ, & H_1, \\ D < TZ, & H_0, \end{cases} \tag{15}$$

where H_1 indicates that the target is detected, H_0 means that no target is detected, D stands for detection statistics value, T is the normalization factor, and Z represents the estimated power of interference and noise. It is assumed that only Gaussian white noise exists in the echo data of airborne PAR except DP signals and multipath signals, and interference and sea clutter are suppressed during the MTD operation in Figure 1.

In the process of CA-CFAR [28], the relationship between false alarm probability P_{fa} and normalization factor T is as follows:

$$P_{fa} = \int_0^\infty e^{-s/\mu} f_S(s) ds = \int_0^\infty e^{-s/\mu} \mu^{-N} s^{N-1} e^{-s/\mu} ds = \left(1 + \frac{T}{N}\right)^{-N}. \tag{16}$$

Therefore, when the P_{fa} is fixed, the normalization factor T can be represented as follows:

$$T = N\left(P_{fa}^{-1/N} - 1\right), \tag{17}$$

where $N = 2n$ is the number of reference cell.

The electromagnetic echo signal can be regarded as a sinusoidal sequence [24]. The detection probability expression P_d of the proposed incoherent integration detection method can be represented as follows:

$$\begin{aligned} P_d &= \int_{S'}^\infty \frac{1}{2\mu} \left(\frac{z}{\lambda'}\right)^{n'-2/4} e^{-z+\lambda'/2\mu} I_{n'/2-1}\left(\frac{\sqrt{z\lambda'}}{\mu}\right) dz \\ &= Q_M\left(\sqrt{2\lambda'}, \sqrt{2S'}\right) + e^{-(S'+\lambda')} \left(\frac{S'}{\lambda'}\right)^{1/2} I_1\left(2\sqrt{\lambda' S'}\right), \end{aligned} \tag{18}$$

where $S' = T/N \sum_{i=1}^{N} X_i \approx T\mu$ is the detection threshold, μ is the background noise power, $n' = 2N$, $\lambda' = P_{o\_di}/\mu = (1 + |\rho|^2) P_{o\_d}/\mu^2$, $Q_M(\cdot)$ is the Q function of Marcum [28], and $I_1(\cdot)$ is the modified Bessel function of first order. The derivation of equation (18) is detailed in the Appendix.

4. Simulation Results

The SMRC characteristics of the DP signal and the multipath signal are analyzed, and the effectiveness of the proposed incoherent integration detection method is verified. Finally, the influence of the SMRC ρ and false alarm probability P_{fa} on detection probability is discussed, respectively.

The transmitting and receiving of airborne PAR systems are in phased array mode. For convenience, the amplitude-phase error and mutual coupling effect of the airborne PAR system are not considered. All the results in this section are simulated by MATLAB software.

Table 1 shows the main system parameters of airborne PAR.

In Table 1, the receiving antenna M refers to the number of antennas in the elevation direction. Since the reflection area is on the calm sea surface, only the strong specular multipath phenomenon needs to be considered, and the height of reflection area is h_b = 20m. According to Table 1, a range bin represents 75 m.

Simulation 1: the DP range R_d belongs to [10, 40]km, and Figure 4 shows the relationship between the angle θ_B and the DP range R_d.

In Figure 4, when DP range belongs to [10, 40]km and H is 1 km, 1.5 km, 2 km, and 2.5 km, respectively, the minimum range bin differences between the multipath signal and the DP signal are 16, 24, 32, and 40, respectively.

Taking the ground-based radar as a comparative experiment, it is assumed that the platform height of the ground-based radar is only 50 m, and other parameters of the ground-based radar are the same as those in Table 1. When the DP range belongs to [10, 40]km, angle θ_B of the ground-based radar does not exceed 0.22 degree and the maximum range bin difference between the multipath signal and the DP signal is less than 1. Obviously, the angle θ_B of the airborne PAR is much larger than that of the ground-based radar, and the multipath signal and the DP signal of the airborne PAR are in different range bins.

According to the measured RCS data which has been provided in [24], it can be seen that the SMRC amplitude $|\rho|$ is possible to be more than 1 at such a large angle θ_B of airborne PAR, which means that the SMRC characteristics introduced previously are in line with the actual situation. Therefore, it is important to utilize the energy of multipath signals for signal detection, which is often ignored in current detection methods [21–23].

Simulation 2: since the reflection surface height h_b is an estimated value based on the topography of the reflection surface, the estimated reflection surface height will inevitably lead to a deviation of multipath range estimation in the target pairing process. Assume that the actual height and the calculated height of the reflection surface are $\overline{h}_b$ = 20m and $\widetilde{h}_b$, respectively. $\Delta_R = |\widetilde{R}_{MP} - \overline{R}_{MP}|$, $\Delta_h = |\widetilde{h}_b - \overline{h}_b|$, where $\overline{R}_{MP}$ is the corresponding multipath range in the condition of $\overline{h}_b$ = 20m, and $\widetilde{R}_{MP}$ is the corresponding multipath range when the height of the reflection surface is $\widetilde{h}_b$. Figure 5 simulates the multipath range deviation when the height deviation between the calculated reflection surface and the actual reflection surface changes.

In Figure 5, as Δ_h increases, Δ_R will also increase. But in the case of the same Δ_h, Δ_R will gently decrease with the increase of R_d. It can be seen from Figure 5 that Δ_R is always less than one range bin when $\Delta_h \le 40$m. For the multipath model with the reflection area on the calm sea surface, Δ_h is difficult to exceed 40m, indicating that the reflection surface height deviation has a limited influence on the estimation of multipath range bin.

Simulation 3: the airborne PAR transmits LFM signal, the transmitting time width is 40us, the bandwidth is 1.5MHz, and the pulse repetition frequency is f_r = 2000Hz. Assuming that there are three targets with DP ranges of

Table 1: System parameters.

Description	Symbol	Value
Wavelength	λ	0.03 m
Number of receiving antennas	M	15
Platform height	H	1.5 km
Reflection attenuation coefficient	ε	1
Earth radius	R_e	6375 km
Direct path direction	θ_d	50°
Multipath direction	θ_i	−54.11°
Sampling frequency	f_s	2 MHz

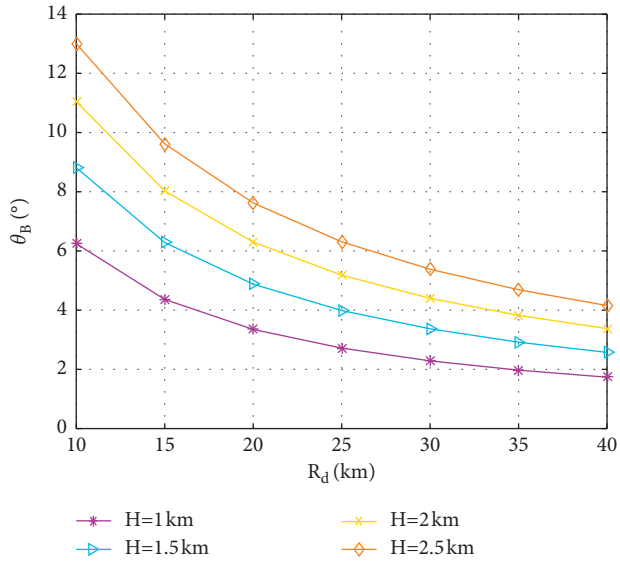

Figure 4: The relationship between the angle θ_B and the DP range R_d.

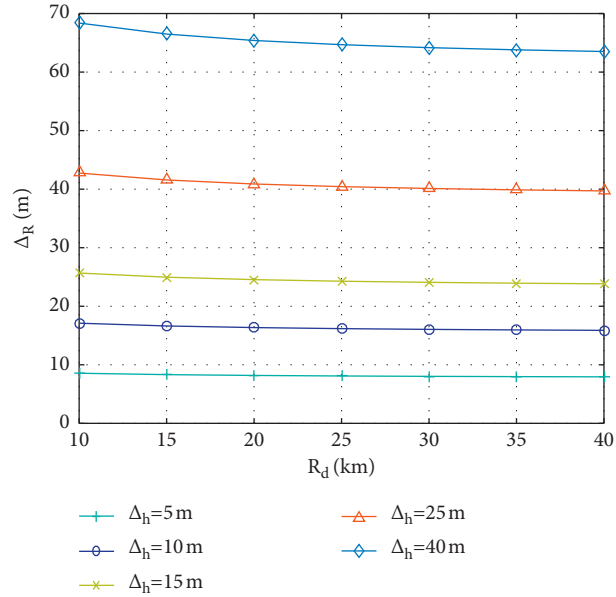

Figure 5: The relationship between multipath range deviation and reflection surface deviation.

24.25 km, 25 km, and 25.9 km, respectively, we set the SNR after PC to SNR = 12dB, the number of guard cells taken is 1, and the reference cell as follows: $N = 16$, $P_{fa} = 10^{-6}$, and $\rho = -1.2$. Figure 6 compares the output gain of conventional CA-CFAR with that of the proposed incoherent integration detection method.

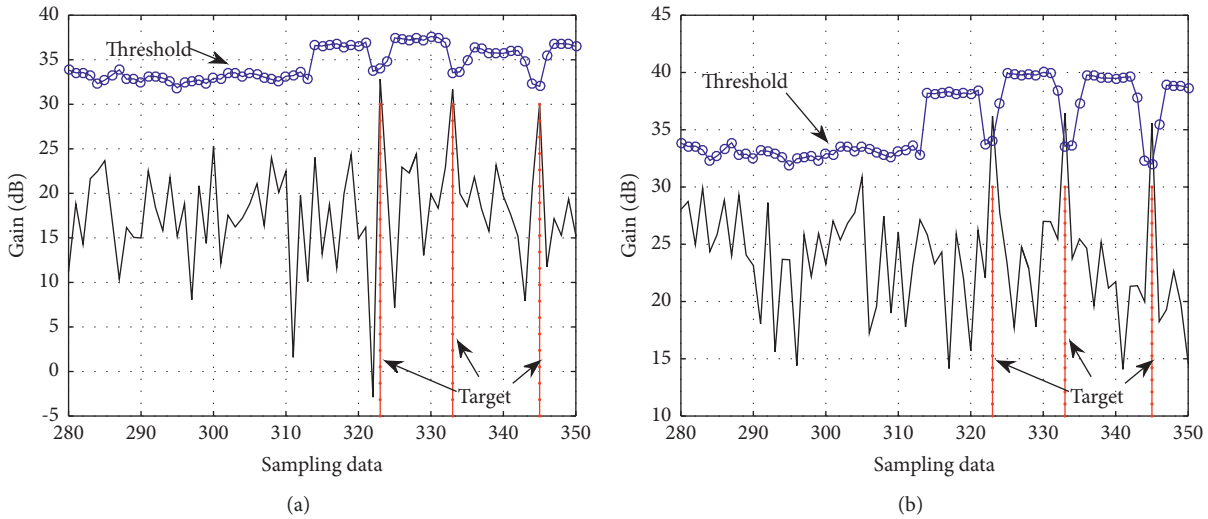

Figure 6: Comparison of output gain amplitude. (a) The gain of CA-CFAR. (b) The gain of the proposed incoherent integration detection method.

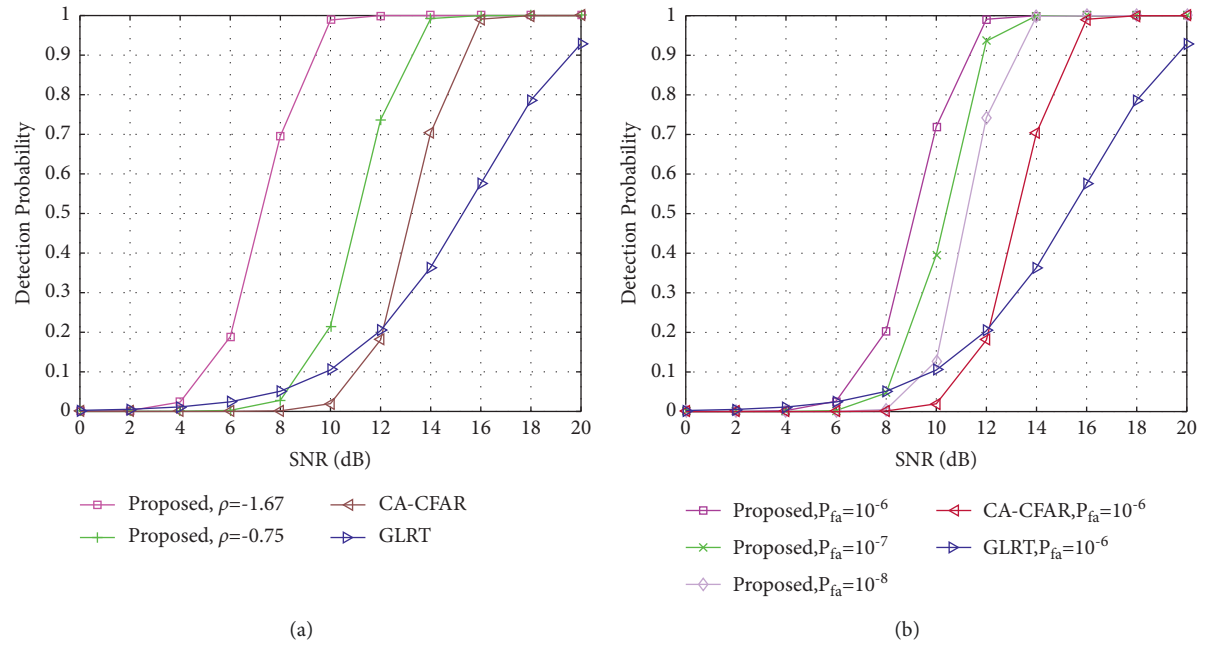

Figure 7: Comparison of detection probability. (a) Detection probability of different ρ, when $P_{fa} = 10^{-6}$. (b) Detection probability of different P_{fa}, when $\rho = -1.2$.

In Figure 6, the DP range bins of three targets are at the 323th, 333th, and 345th sampling data, and the method in Figure 6(b) is the proposed method. The target output gains of CA-CFAR are 32.84 dB, 31.67 dB, and 30 dB, respectively, and the target output gains of the proposed method are 36.19 dB, 36.46 dB, and 35.57 dB, respectively. From Figure 6, the target output gains of the proposed incoherent integration method are larger than the CA-CFAR, and the proposed method can successfully pass the detection threshold at the DP range bins, but the CA-CFAR method cannot. In fact, according to the previous analysis, the proposed method makes use of the return energy of multipath data, so the proposed method is more likely to pass the detection threshold.

Simulation 4: the CA-CFAR and GLRT [28, 30] methods are used as comparison results. Supposing $R_d = 25$km and $\sigma_i/\sigma_d \in [0.8, 4]$, we can calculate the SMRC belongs to $\rho \in [-1.67, -0.75]$. Figure 7(a) shows the influence of the SMRC $\rho = [-1.67, -0.75]$ when $P_{fa} = 10^{-6}$, and Figure 7(b) shows the influence of false alarm probability $P_{fa} = [10^{-6}, 10^{-7}, 10^{-8}]$ when $\rho = -1.2$.

In Figure 7, the CA-CFAR and GLRT methods directly detect the signal of the DP range bin. From Figures 7(a) and 7(b), it is obvious that the proposed incoherent integration

detection method makes full use of the energy of the multipath signal, so it has good detection probability performance.

In summary, Figure 4 demonstrates the special multipath phenomenon of airborne PAR, that is, multipath power of airborne PAR may be greater than the DP power, Figure 5 analyzes the influence of the reflection surface height deviation on the estimation multipath range deviation, Figure 6 demonstrates that the proposed method can work with multiple targets, and Figure 7 shows the detection probability performance of the proposed method.

5. Conclusions

This paper analyzes the SMRC characteristics of airborne PAR in a multipath environment. Based on these characteristics, an incoherent integration detection method is proposed, which makes full use of the energy of multipath signals. At the same time, the detection probability of incoherent integration in the multipath environment is given. The proposed detection process and simulation conditions are in line with the practical application. Finally, simulation results show that the proposed method can improve the detection performance.

However, accurate prior information is required in the target pairing process. When the prior information is inaccurate, the success probability of the target pairing process will decrease. Therefore, solving the dependence of the target pairing process on prior information is the focus of future research.

Appendix

The echo signal can be written as follows:

$$s(n) = a\ \cos(w_0 n + \phi_0), \tag{19}$$

where the envelope a is a constant, ϕ_0 is the initial phase, and n is a discrete sequence. Then,

$$s(n) = a\ \cos(\phi_0)\cos(w_0 n) - a\ \sin(\phi_0)\sin(w_0 n). \tag{20}$$

The Gaussian noise sequence can be written as follows:

$$N(n) = n_I(n)\cos(w_0 n) - n_Q(n)\sin(w_0 n). \tag{21}$$

The signal sequence can be written as follows:

$$\begin{aligned} N'(n) &= s(n) + N(n) \\ &= \left[a\ \cos(\phi_0) + n_I(n)\right]\cos(w_0 n) \\ &\quad - \left[a\ \sin(\phi_0) + n_Q(n)\right]\sin(w_0 n) \\ &= A_I(n)\cos(w_0 n) - A_Q(n)\sin(w_0 n). \end{aligned} \tag{22}$$

The square of the $N'(n)$ envelope is as follows:

$$\begin{aligned} A^2(n) &= A_I^2(n) + A_Q^2(n) = \left[a\ \cos(\phi_0) + n_I(n)\right]^2 \\ &\quad + \left[a\ \sin(\phi_0) + n_Q(n)\right]^2. \end{aligned} \tag{23}$$

The output after incoherent integration is as follows:

$$V' = \left[\sum_{i=1}^{m}\left(\underbrace{a\ \cos(\phi_0) + n_{Ii}}_{V_{Ii}'}\right)^2 + \sum_{i=1}^{m}\left(\underbrace{a\ \sin(\phi_0) + n_{Qi}}_{V_{Qi}'}\right)^2\right], \tag{24}$$

where m is the sequence length and n_{Ii} and n_{Qi} are the noise components at i time, $n_{Ii}, n_{Qi} \sim \mathcal{N}(0, \sigma^2)$. Let $a_I = a\ \cos(\phi_0)$, $a_Q = a\ \sin(\phi_0)$, so $V_{Ii}' \sim \mathcal{N}(a_I, \sigma^2)$, $V_{Qi}' \sim \mathcal{N}(a_Q, \sigma^2)$. The probability density functions of $Y_{Ii} = (V_{Ii}')^2$ and $Y_{Qi} = (V_{Qi}')^2$ are as follows:

$$f_{Y_{Ii}}(y_{Ii}) = \frac{1}{\sqrt{2\pi\sigma^2 y_{Ii}}}\left[e^{-\frac{\left(\sqrt{y_{Ii}} - a_I\right)^2}{2\sigma^2}} + e^{-\frac{\left(-\sqrt{y_{Ii}} - a_I\right)^2}{2\sigma^2}}\right], \tag{25}$$

$$f_{Y_{Qi}}(y_{Qi}) = \frac{1}{\sqrt{2\pi\sigma^2 y_{Qi}}}\left[e^{-\frac{\left(\sqrt{y_{Qi}} - a_Q\right)^2}{2\sigma^2}} + e^{-\frac{\left(-\sqrt{y_{Qi}} - a_Q\right)^2}{2\sigma^2}}\right]. \tag{26}$$

For $f_{Y_{Ii}}(y_{Ii})$ of equation (25), we can rewrite as follows:

$$f_{Y_{Ii}}(y_{Ii}) = \frac{1}{\sqrt{2\pi\sigma^2 y_{Ii}}} e^{-(y+a^2)/2\sigma^2}\cosh\left(\frac{a_I\sqrt{y_{Ii}}}{\sigma^2}\right), \tag{27}$$

where $2\cosh(b) = e^b + e^{-b}$. The characteristic function of Y_{Ii} is as follows:

$$Q_{Y_{Ii}}(u) = \frac{1}{\sqrt{1 - j2\sigma^2 u}} e^{-a_I^2/2\sigma^2 + a_I^2/2\sigma^2\left(1 - j2\sigma^2 u\right)}, \tag{28}$$

where $j = \sqrt{-1}$. Since Y_{Ii} is independent and identically distributed, the characteristic function of $Y_{Ii}'' = \sum_{i=1}^{m} Y_{Ii}$ is as follows:

$$Q_{Y_{Ii}''}(u) = \prod_{i=1}^{m} Q_{Y_{Ii}'}(u) = \left(\frac{1}{1 - j2\sigma^2 u}\right)^{m/2} e^{-ma_I^2/2\sigma^2 + ma_I^2/2\sigma^2 (1 - j2\sigma^2 u)}. \tag{29}$$

Carrying out the inverse Fourier transform of equation (29), the probability density function of Y_{Ii}'' can be obtained as follows:

$$f_{Y_{Ii}''}(y_{Ii}'') = \frac{1}{2\sigma^2}\left(\frac{y_{Ii}''}{(\lambda_I')^2}\right)^{m-2/4} e^{-(\lambda_I' + y_{Ii}'')/2\sigma^2} I_{m/2-1}\left(\frac{\sqrt{y_{Ii}''\lambda_I'}}{\sigma^2}\right), \tag{30}$$

where $\lambda_I' = a_I^2 N/\sigma^2$, $y_{Ii}'' \geq 0$, and $I_{n'}(\cdot)$ is the first modified Bessel function of order n'.

In the same way, the probability density function of $Y_{Qi}'' \geq 0 = \sum_{i=1}^{m} Y_{Qi}$ can be obtained as follows:

$$f_{Y_{Qi}''}(y_{Qi}'') = \frac{1}{2\sigma^2}\left(\frac{y_{Qi}''}{(\lambda_Q')^2}\right)^{m-2/4} e^{-(\lambda_Q' + y_{Qi}'')/2\sigma^2} I_{m/2-1}\left(\frac{\sqrt{y_{Qi}''\lambda_Q'}}{\sigma^2}\right), \tag{31}$$

where $\lambda_Q' = a_Q^2 N/\sigma^2$, $y_{Qi}'' \geq 0$. According to equations (24), (30), and (31), the probability density function of V' can be obtained as follows:

$$f_{V'}(v') = \frac{1}{2\sigma^2}\left(\frac{v'}{\lambda'^2}\right)^{m-2/4} e^{-(\lambda' + v')/2\sigma^2} I_{m/2-1}\left(\frac{\sqrt{v'\lambda'}}{\sigma^2}\right), \tag{32}$$

where $\lambda' = \lambda_I' + \lambda_Q'$, $v' \geq 0$. Then, with the help of the derivation ideas in [31, 32], we can obtain the detection probability of V' as follows:

$$\begin{aligned} P_d &= \int_S^{\infty} f_{V'}(v')dv' \\ &= Q_M\left(\sqrt{2\lambda'}, \sqrt{2S}\right) + e^{-(S+\lambda')}\left(\frac{S}{\lambda'}\right)^{1/2} I_1\left(2\sqrt{\lambda' S}\right), \end{aligned} \tag{33}$$

where the expression of Marcum's Q function $Q_M(\sqrt{2\lambda'}, \sqrt{2S})$ is as follows:

$$Q_M\left(\sqrt{2\lambda'}, \sqrt{2S}\right) = \int_{\sqrt{2S}}^{+\infty} te^{-(\lambda' + S)} I_0\left(\sqrt{2\lambda'}\, t\right)dt. \tag{34}$$

Data Availability

The data used to support the findings of this study are available from the corresponding author upon request.

Conflicts of Interest

The authors declare that they have no conflicts of interest.

Acknowledgments

This work was partially supported by the Fund for Foreign Scholars in University Research and Teaching Programs (the 111 Project) (no. B18039).

References

[1] J. Brown, K. Woodbridge, A. Stove, and S. Watts, "Air target detection using airborne passive bistatic radar," *Electronics Letters*, vol. 46, no. 20, pp. 1396-1397, 2010.

[2] Z. Wang, S. Shi, Z. Cheng, and Z. He, "A modified sequential multiplexed method for detecting airborne and sea targets with over-the-horizon radar," *IEEE Access*, vol. 8, pp. 84082–84092, 2020.

[3] A. Hussain, I. Hussain, and I. Mir, "Target parameter estimation in reduced dimension STAP for airborne phased array radar," *IEEE International Multitopic Conference (INMIC)*, vol. 20, pp. 1–6, 2020.

[4] D. Fu, J. Wen, J. Xu, G. Liao, and S. Ouyang, "STAP-based airborne radar system for maneuvering target detection," *IEEE Access*, vol. 7, pp. 62071–62079, 2019.

[5] R. Cheng, X. Liang, F. Zhang, and L. Chen, "Multipath scattering of typical structures in urban areas," *IEEE Transactions on Geoscience and Remote Sensing*, vol. 57, no. 1, pp. 342–351, 2019.

[6] Z. Wang, Z. He, and Q. He, "GLRT detectors for airborne radar based on knowledge-aided and compressive sensing," *IEEE International Geoscience and Remote Sensing Symposium*, vol. 23, pp. 2221–2224, 2019.

[7] S. H. Gulen Yilmaz and H. Taha Hayvaci, "Multipath exploitation radar with adaptive detection in partially homogeneous environments," *IET Radar, Sonar & Navigation*, vol. 14, no. 10, pp. 1475–1482, 2020.

[8] Z. Zhang, B. Chen, and M. Yang, "Moving target detection based on time reversal in a multipath environment," *IEEE Transactions on Aerospace and Electronic Systems*, vol. 57, no. 5, pp. 3221–3236, 2021.

[9] H. T. Hayvaci, A. De Maio, and D. Erricolo, "Improved detection probability of a radar target in the presence of multipath with prior knowledge of the environment," *IET Radar, Sonar & Navigation*, vol. 7, no. 1, pp. 36–46, 2013.

[10] R. Yang, Y. Bar-Shalom, and G. W. Ng, "Altitude estimation using multipath with a two-dimensional radar over spherical earth," *IEEE Transactions on Aerospace and Electronic Systems*, vol. 54, no. 2, pp. 770–782, 2018.

[11] X. Yang, H. Zhang, and Q. Luo, "Multi-path interference analysis and simulation of secondary surveillance radar for civil aviation ATC," *IEEE Information Tech., Networking, Elec. and Automation Control Conf. (ITNEC)*, vol. 1, pp. 1164–1168, 2020.

[12] Y. Hu, Y. Zhao, S. Chen, and X. Pang, "Direction of arrival estimation of airborne multiple-input multiple-output radar in multipath environment," *IET Radar, Sonar & Navigation*, vol. 15, no. 10, pp. 1173–1180, 2021.

[13] H. Tang, X. Wan, and Y. Liu, "On the performance of multipath in reference signal for passive radar interference cancellation," in *Proceedings of the IEEE Radar Conference*, pp. 1313–1316, Washington, D.C., WA, USA, 2017.

[14] G. Galati, G. Pavan, and C. Wasserzier, "Environmental effects on ground-based radar measurements," in *Proceedings of*

the IEEE 5th International Workshop on Metrology for AeroSpace, pp. 349–354, Torino, Italy, June 2019.

[15] D. J. Rabideau, "Clutter and jammer multipath cancellation in airborne adaptive radar," *IEEE Transactions on Aerospace and Electronic Systems*, vol. 36, no. 2, pp. 565–583, 2000.

[16] O. Rabaste and D. Poullin, "Rejection of doppler shifted multipaths in airborne passive radar," in *Proceedings of the IEEE Radar Conference*, pp. 1660–1665, Arlington, VA, USA, March 2015.

[17] D. Bonacci, F. Vincent, and B. Gigleux, "Robust DOA estimation in case of multipath environment for a sense and avoid airborne radar," *IET Radar, Sonar & Navigation*, vol. 11, no. 5, pp. 797–801, 2017.

[18] J. G. Teti, "Wide-band airborne radar operating considerations for low-altitude surveillance in the presence of specular multipath," *IEEE Transactions on Antennas and Propagation*, vol. 48, no. 2, pp. 176–191, 2000.

[19] Y. Liu, B. Jiu, X.-G. Xia, H. Liu, and L. Zhang, "Height measurement of low-angle target using MIMO radar under multipath interference," *IEEE Transactions on Aerospace and Electronic Systems*, vol. 54, no. 2, pp. 808–818, 2018.

[20] J. Tan, Z. Nie, and S. He, "A novel precise angle measurement for meter-wave radar based on multipath cancellation," in *Proceedings of the CIE International Conference on Radar*, pp. 1–4, Guangzhou, China, July 2016.

[21] M. Fazlollahpoor, M. Derakhtian, and S. Khorshidi, "Passive MIMO radar detection in the presence of clutter or multi-path without reference channel," *IET Radar, Sonar & Navigation*, vol. 15, no. 2, pp. 154–166, 2021.

[22] A. Aubry, A. De Maio, G. Foglia, and D. Orlando, "Diffuse multipath exploitation for adaptive radar detection," *IEEE Transactions on Signal Processing*, vol. 63, no. 5, pp. 1268–1281, 2015.

[23] Y. Rong, A. Aubry, and A Tang, "Diffuse multipath exploitation for adaptive detection of range distributed targets," *IEEE Transactions on Signal Processing*, vol. 68, pp. 1197–1212, 2020.

[24] M. I. Skolnik, *Radar Handbook*, McGraw-Hill, New York, USA, 1990.

[25] H. Xiang, B. Chen, and M. Yang, "Altitude measurement based on characteristics reversal by deep neural network for VHF radar," *IET Radar, Sonar & Navigation*, vol. 13, no. 1, pp. 98–103, 2018.

[26] B. Chen, G. Zhao, and S. Zhang, "Altitude measurement Based on beam split and frequency diversity in VHF radar," *IEEE Transactions on Aerospace and Electronic Systems*, vol. 46, no. 1, pp. 3–13, 2010.

[27] H. Xiang, B. Chen, T. Yang, and D. Liu, "Improved de-multipath neural network models with self-paced feature-to-feature learning for DOA estimation in multipath environment," *IEEE Transactions on Vehicular Technology*, vol. 69, no. 5, pp. 5068–5078, 2020.

[28] M. A. Richards, *Fundamentals of Radar Signal Processing*, McGraw-Hill, New York, USA, 2014.

[29] C. Liu, Y. Liu, and Q. Li, "Radar target MTD 2D-CFAR algorithm based on compressive detection," *IEEE International Conference on Mechatronics and Automation (ICMA)*, vol. 32, pp. 83–88, 2021.

[30] Z. Shang, X. Li, Y. Liu, Y. Wang, and W. Liu, "GLRT detector based on knowledge aided covariance estimation in compound Gaussian environment," *Signal Processing*, vol. 155, pp. 377–383, 2019.

[31] L. Wang, J. Tang, and Q. Liao, "A study on radar target detection based on deep neural networks," *IEEE Sensors Letters*, vol. 3, no. 3, pp. 1–4, 2019.

[32] S. Fortunati, L. Sanguinetti, F. Gini, M. S. Greco, and B. Himed, "Massive MIMO radar for target detection," *IEEE Transactions on Signal Processing*, vol. 68, pp. 859–871, 2020.